J. P. Gudas, G. R. Irwin†, R. W. Armstrong†, and X. J. Zhang†*

A Model for Transition Fracture of Structural Steels from Observations of Isolated Cleavage Regions

REFERENCE Gudas, J. P., Irwin, G. R., Armstrong, R. W., and Zhang, X. J., **A model for transition fracture of structural steels from observations of isolated cleavage regions**, *Defect Assessment in Components – Fundamentals and Application*, ESIS/EGF9 (Edited by J. G. Blauel and K.-H. Schwalbe) 1991, Mechanical Engineering Publications, London, pp. 549–568.

ABSTRACT Near upper shelf cleavage initiations in ASTM A-710 Grade A steel were examined. Metallographic and fractographic results were obtained of isolated cleavage regions in precracked and side-grooved Charpy 'V' notch (CVN) specimens. The clearly identified cleavage origins were associated with localised hole-joining failures in clumps of tempered martensite–austenite (M–A) or tempered bainitic carbide clusters. A three stage model is postulated to trigger cleavage fracture in the CVN near-upper region as follows: (I) irregularities of abrupt plastic deformation and preceding crack separation combine with the crack tip stresses to provide local regimes of high tensile stress acting on particle clumps; (II) quick separation of a particle clump occurs after relatively small uniform strain, giving very rapid load transfer to the adjacent ferrite, and; (III) spreading of cleavage in the ferrite is initiated from a suitably oriented cleavage embryo experiencing the cumulative, extremely large values of normal stress that are transmitted. A main feature of this three stage model is to appropriately address the rare event nature of cleavage initiation in the upper transition temperature regime of fracturing behaviour. The results of this investigation point to the role of particle clumps as initiation regions for cleavage fracture if appropriate local conditions of stress elevation are met. The existence of microstructural inhomogeneity provides the setting for cleavage to occur under conditions otherwise favouring a totally ductile fracturing process.

Introduction

Cleavage initiation in structural steels, across the transition temperature range, can be regarded as a three stage sequence of local stress elevations. In this general model, the highly localised rapid brittle separation of a particle or of a particle clump is included in stage II. Preceding this in Stage I, at a larger size scale, are the local stress elevations of various magnitude which occur due to the common irregularities of slip and crack separation. An adequately rapid–brittle fracture of a particle or particle clump is most likely when driven by the largest of these local stress elevations. Thus Stage I behaviours are of major importance relative to the scatter of small specimen toughness measurements commonly observed in the transition temperature range. Fractures of particles or particle clumps are not crystallographic. Thus, for completeness, there must be a stage III in which the added stress elevation from stage II causes formation and spreading of cleavage from a minute cleavage embryo in the adjacent ferrite matrix. These comments formalise ideas previously explored using scanning electron microscopy (SEM) studies of cleavage initiation in nuclear

* David Taylor Research Centre, Annapolis, Maryland, USA.
† Department of Mechanical Engineering, University of Maryland, College Park, Maryland, USA.

vessels steels and their weld metals (1)–(3). In this paper, application of the above model is extended using isolated cleavage fractures of ASTM A-710 Grade A steel.

McMahon and Cohen (4) used plastic film replicas during interrupted loading of thin steel-plate tensile specimens to examine small cleavage cracks which had formed and arrested. They found that cracks in carbide films or plates in grain boundaries acted as sources for cleavage in the adjacent ferrite. It was natural for subsequent investigations and modelling of cleavage initiation in steels to focus mainly on individual carbide or inclusion particle fractures. In addition, illustrative experiments often used temperatures on the lower shelf of the fracture transition where the influence of stage I is relatively small. Smith (5) developed a 'static' model for cleavage crack initiation which included a dislocation pile-up contribution to the crystal scale process of crack nucleation, and assumed a plastic work term to propagate a crack into the ferrite that was significantly higher than the plastic work term for cleavage crack initiation in a hard particle. Knott (6) examined the deformation and fracture of notched and smooth specimens of two C–Mn steels and concluded that a critical stress criterion existed for cleavage fracture provided that yield had first occurred. Ritchie, Knott, and Rice (7) developed a correlation of the critical value of the tensile stress for unstable cleavage related to the attainment of a maximum principal stress over a critical distance ahead of the crack tip. The key feature of this model was the introduction of a size scale over which the critical stress criterion must be met. Evaluation of the microstructural significant distance led Curry and Knott (8) to conclude that cleavage fracture is likely to be initiated by the largest carbide particle found in the crack tip region subject to stress elevation. Further, the actual site for initiation was likely to be determined by competition between smaller carbide particles in a small region of higher stress and less numerous larger carbides in a larger region of lower critical stress. Curry and Knott (9) subsequently concluded that the 95th percentile carbide size is a reasonable estimate of the crack nucleus size for cleavage fracture in spherodized tool steels. Later models (10)–(14) were developed under assumptions of statistically distributed carbide particle sizes and weakest link statistics applied to particles located in the plastic zones that were assumed to be cracked. Petch and Armstrong (15) have recently proposed an important role for work hardening to link initial yield strength and fracture toughness measurements of various steels and connected this consideration with the various microstructures studied in these previous investigations.

Stress elevation due to a notch or precrack, constraint, and loading rate are notional features of models which have been addressed to brittle fracture in the lower shelf regime. Where these models include fracture or separation of a particle, the analyses assume local region separations and stress levels consistent with spreading of a Griffith crack in a crystallographic or quasi-crystallographic ferrite matrix. The process which converts an arbitrarily

oriented crack through a glassy particle into a crystallographic separation of comparable size in the ferrite matrix is neglected in these models.

This investigation examined application of the three stage model to cleavage in a high strength ferritic steel in the near upper-shelf regime. Experiments were conducted on ASTM A 710 Grade A Class 3 steel which was austenitised and then quenched at three different rates, followed by ageing which precipitation-strengthened the ferrite and tempered the secondary transformation products. Charpy impact toughness tests were conducted using both precracked specimens and modified specimens containing side-grooves. The latter were utilised in order to increase the constraint along the crack front and to promote flat tensile plastic tearing prior to cleavage. Metallographic and fractographic examinations were conducted with particular emphasis given to examining the fracture processes at the transition from tearing to cleavage fracture in order to identify isolated cleavage regions (ICRs) observed at the fracture transition. The ICR is seen as a 'subcritical' cleavage event which, because it does not contain reinitiation complexities, allows unambiguous identification of the small locus of cleavage initiation.

Material

Table 1 presents the chemical composition of the 19 mm thick ASTM A-710 steel plate which was evaluated, and Table 2 presents the room temperature tensile mechanical properties of this plate in the as-received (Grade A Class III) condition. Three plates measuring 457 mm × 457 mm were removed from the parent plate and were austenitised at 900°C for 1 hour, then quenched in water, oil, or still air. Ageing was accomplished by heating the plates at 650°C for 1 hour, followed by water quench. These heat treatments were designed to vary the ferrite grain size and the amount and size distribution of carbon-rich secondary transformation products which consist mainly of tempered martensite–austenite or tempered bainite (16) and, as much as possible, to reduce differences in strength.

Figure 1 presents light micrographs of the ASTM A-710 steel following the controlled quenching and ageing heat treatments. These photomicrographs were produced with a Picral/Nital etch to highlight the ferrite microstructure and identify the tempered secondary transformation products. Quantitative metallographic analysis indicated that the water-quenched plate contains 35.8

Table 1 Chemical composition of ASTM A-710 steel (wt%)

Material	*C*	*Mn*	*P*	*S*	*Ni*	*Cr*	*Mo*	*Cu*	*Si*
ASTM A-710 specification	0.07 Max.	0.40–0.70	0.025 Max.	0.025 Max.	0.70–1.00	0.60–0.90	0.15–0.25	1.00–1.30	0.40 Max.
Material code GHW	0.041	0.56	0.008	0.004	1.04	0.93	0.19	1.24	0.33

Table 2 Microstructural and mechanical properties of ASTM A-710 grade A steel following controlled quenching and ageing heat treatments

Heat Treatment	Volume Fraction Acicular Ferrite (%)	Volume Fraction Aged M–A or Bainite (%)	Average Polygonal Ferrite Grain Size (microns)	Yield Strength (MPa)	Ultimate Tensile Strength (MPa)	Elongation (% in 50 mm)	Elongation (% in 30 mm)	Reduction in Area (%)
Grade A, Class III				515 Min.	585 Min.	20 Min.		—
Water Quench	35.8	2.8	5.1	527	607		30	82
Oil Quench	5.7	3.4	5.6	479	558		32	82
Air Quench	0	3.4	6.3	441	524		33	80

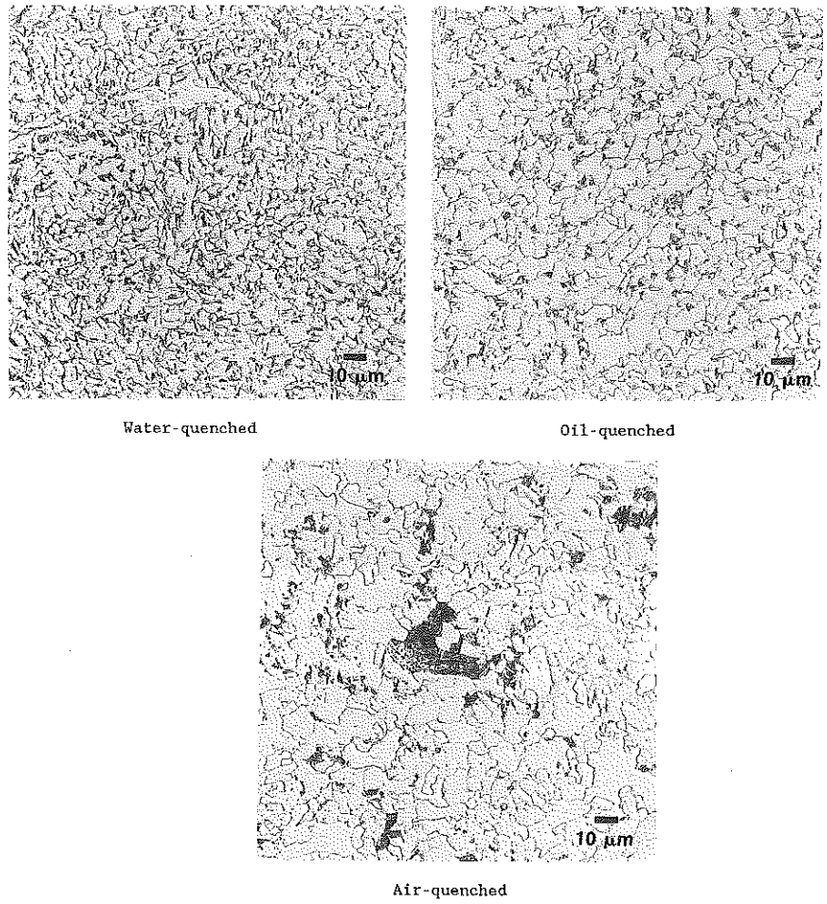

Fig 1 Optical photomicrographs of ASTM A-710 grade A steel following controlled quenching and ageing heat treatments

percent acicular ferrite, 61.4 percent polygonal ferrite, and 2.8 percent tempered M–A. This is consistent with the continuous cooling transformation information presented by Speich and Scoonover **(16)**. The volume of acicular ferrite in the oil-quenched material dropped to 5.7 percent and the air-quenched plate was entirely polygonal ferrite. The polygonal ferrite grain size ranged from 5.1 microns for the water-quenched plate to 6.4 microns for the air-quenched plate. The size of islands of tempered M–A and bainite increased significantly as the quenching rate from austenite was decreased. Figure 2 presents scanning electron micrographs produced from water- and air-quenched specimens which were etched in Picral solution. The individual tempered Fe_3C particles are visible and, for the case of the water-quenched specimen, tended

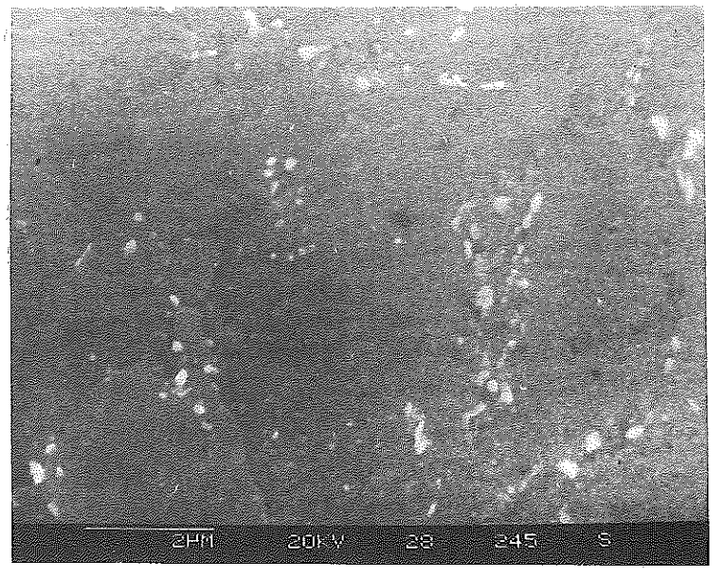

Water-quenched

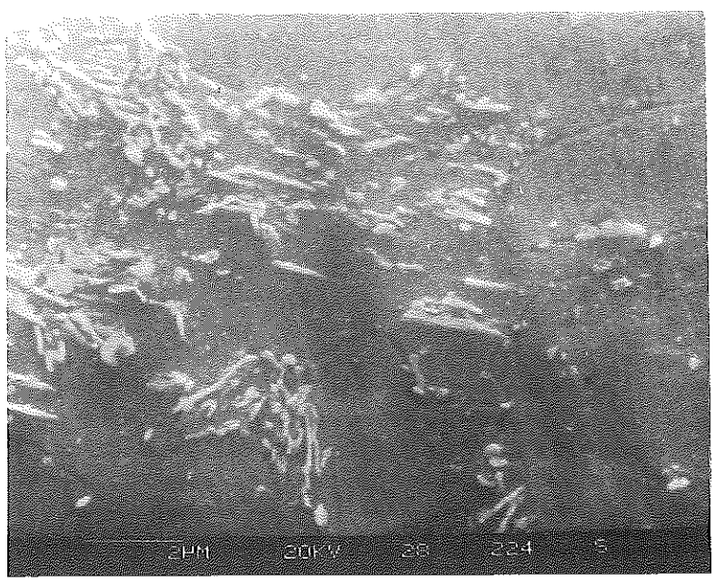

Air-quenched

Fig 2 Scanning electron micrographs of ASTM A-710 grade A steel following water- or air-quenching from austenite followed by ageing

to spherical shapes in accumulations on grain boundaries and triple points. Individual carbides ranging from approximately 0.1 to 0.3 microns in diameter are visible. The air quenched specimen contained elongated tempered carbides which resulted from the slower secondary transformation to bainite. These carbides retained much of their lath or needle shape, and the significantly larger size of the accumulation of such particles is evident. The microstructural characterisation information is summarised in Table 2.

The tensile mechanical properties of the three heat treat conditions are also included in Table 2. The laboratory water-quench material had a yield strength of 527 MPa and exceeded the specification limits for the Grade A Class III condition of ASTM A-710 steel. The oil-quench specimen had a yield strength of 479 MPa and the air-quenched sample exhibited a yield strength of 441 MPa after ageing treatment.

Charpy 'V' notch impact toughness tests

Conventional Charpy impact toughness specimens were produced and precracked to a total crack depth on the order of 40 percent of the original remaining ligament ($a/W = 0.4$). The maximum applied stress intensity for precracking was 25 MPa$\sqrt{\text{m}}$. The net cross section of the side-grooved Charpy impact specimen was the same as the standard specimen described in ASTM E-23, but the width of the specimen was increased to 14 mm to accommodate side grooves to a 2 mm depth on each side, similar to that of the face notch.

Figure 3 presents the Charpy impact toughness results for the three experimental heat treatments produced in this study. In these figures, solid symbols indicate that cleavage was observed in the specimen fracture process. For the case of the precracked CVN specimens, the fracture energy was scaled to allow comparison of both types of specimens on the basis of similar ligament area behind the precrack or notch tip. For all three heat treatments, the precracked specimens produced a narrow temperature range for fracture toughness and fracture mode transitions where specimens failed either by 100 percent ductile fracture, or 100 percent cleavage fracture. The temperature range over which this transition occurred was on the order of 2–5°C. The side-grooved specimens displayed a gradual transition in fracture energy from upper to lower shelf where the fracture surface included a region of ductile fracture followed by a region of cleavage. Table 3 presents a summary of results of the impact toughness tests where the temperature of first observation of cleavage fracture is identified as the CVN transition temperature. The cleavage initiation temperature of the water- and oil-quenched conditions were similar for a given test specimen geometry. The coarse grained microstructure resulting from the air-quench from austenite had measurably higher cleavage transition temperatures in each test. The side-grooved CVN specimens uniformly triggered cleavage at higher temperatures than were observed with the precracked specimens.

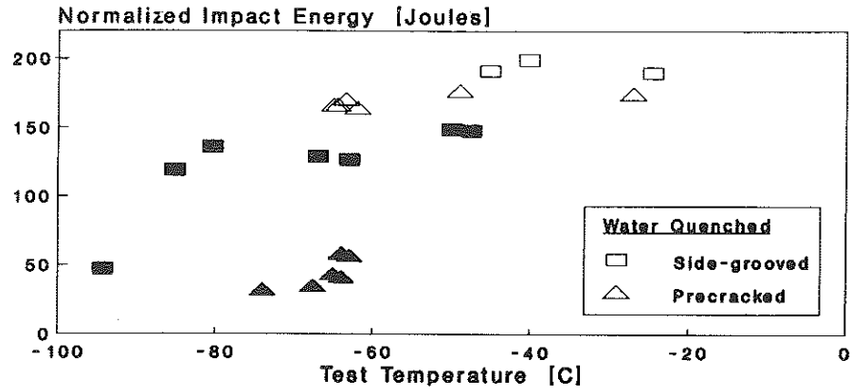

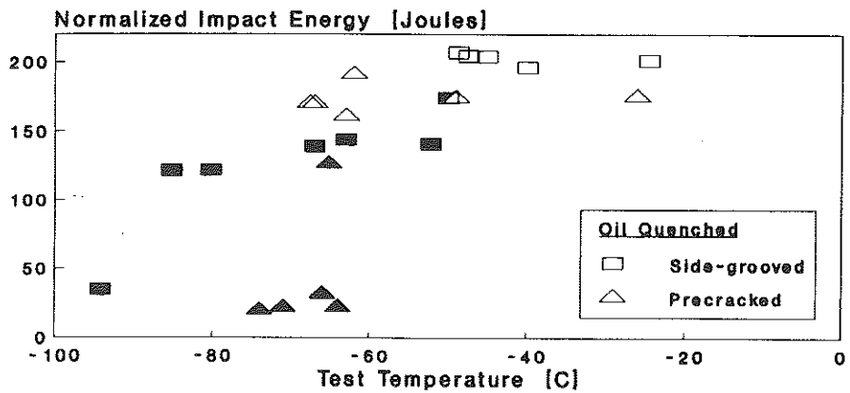

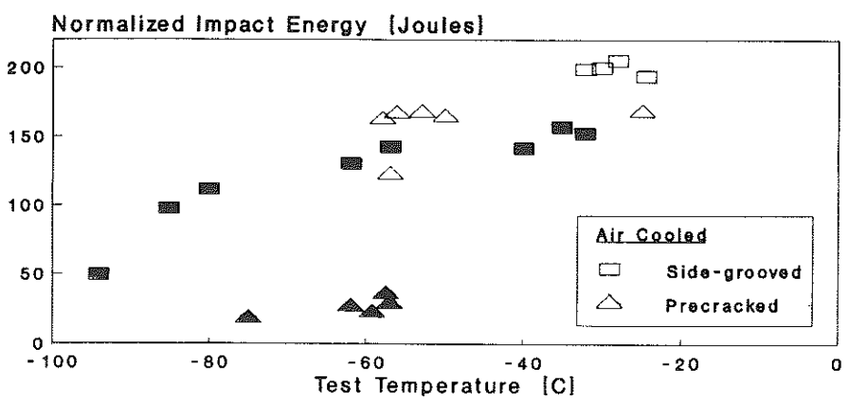

Fig 3 Charpy impact toughness test results for ASTM A-710 grade A steel following controlled quenching and ageing heat treatments (filled symbols denote cleavage fracture)

Table 3 Summary of results of Charpy impact toughness tests of ASTM A-710 grade A steel following controlled quenching and ageing heat treatments

Heat treatment	*Ferrite grain size (microns)*	*0.2 percent yield strength (MPa)*	*CVN transition temperature*	
			Pre-cracked specimens (°C)	*Side-grooved specimens (°C)*
Water quench	5.1	527	−63	−48
Oil quench	5.6	479	−64	−50
Air quench	6.3	441	−57	−32

Fractographic analysis

Metallographic and scanning electron microscope (SEM) fractographic examination of specimens was conducted with particular emphasis given to characterisation of the fracture processes which occurred at the transition from tearing to cleavage fracture. Following the work of Zhang *et al.* **(1)**, attempts were made to identify isolated cleavage regions (ICRs) observed at the fracture transition. Stereographic pairs of ICRs were produced, as were high resolution fractographs of apparent sites of cleavage initiation.

A special technique of stereo SEM section fractography was employed in this study to observe the fracture surface appearance and the microstructure underneath the isolated cleavage regions. After a pair of stereo SEM fractographs were taken on the area of interest, a rough section was made along a line at a distance of 0.1–0.2 mm from the cleavage initiation point. The initiation locus was then approached by cycles of polishing, removal of coating material, checking the sectioning position, and re-coating. When the section was thought to be at or within 1 micron of the initiation locus, the coating material was removed, and the polished section surface was etched. Both the locus region of the fracture surface and the underlying microstructure were simultaneously examined by using stereo SEM imaging.

For the case of the precracked CVN specimens, there was no evidence of a zone of plastic tearing preceding cleavage. This fracture process contained only a stretch zone, which was followed by either entirely ductile (hole-joining) fracture, or entirely cleavage fracture. Examination of specimens from each heat treatment did not reveal 'isolated cleavage regions' with the precracked specimens.

In side-grooved CVN specimens which exhibited plastic (hole-joining) fracture followed by cleavage, several isolated cleavage regions were found just prior to the region of massive cleavage. However, distinct from the earlier work of Zhang *et al.* **(1)** and Irwin *et al.* **(2)**, the observations of ICRs in this fine-grained ferritic steel were very limited. Figure 4 is a scanning electron fractograph of an ICR which occurred at the interface between tearing and cleavage fracture in a water-quenched specimen which contained a substantial

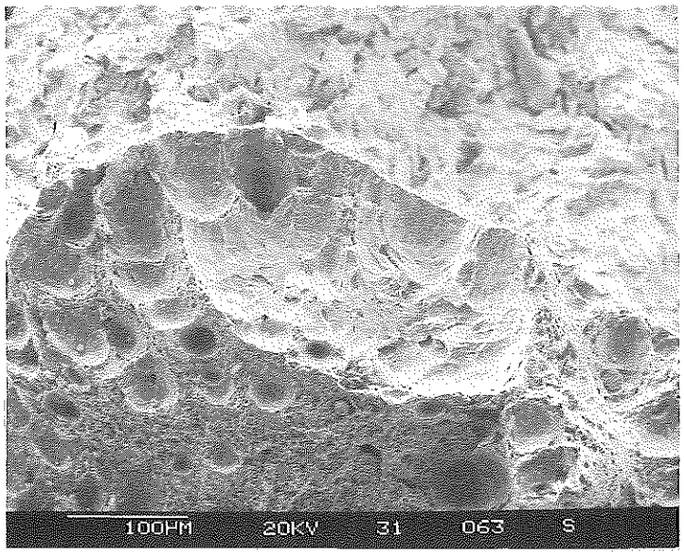

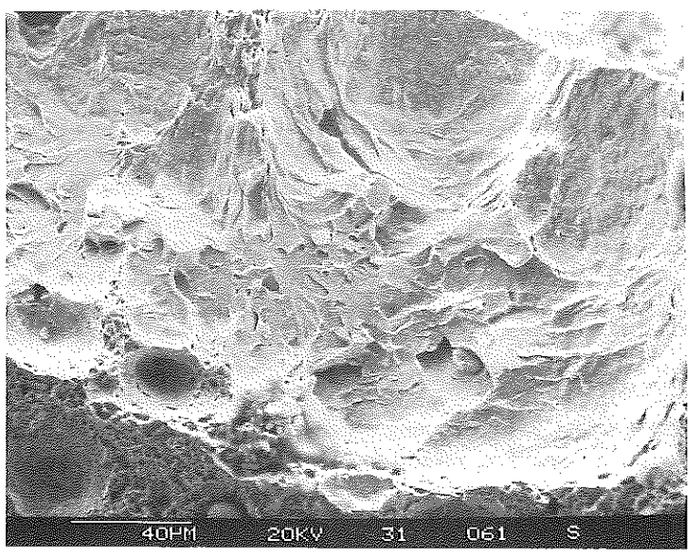

Fig 4 Scanning electron fractographs of isolated cleavage region in water-quenched and aged ASTM A-710 grade A steel side-grooved CVN test specimen

portion of acicular ferrite. Here, it can be seen that the region of cleavage fracture was entirely surrounded by hole joining. This ICR is approximately 40 microns wide. Careful fractographic examination did not reveal a broken particle as source, but rather pointed to what is apparently a clump of tempered M–A, Fig. 5.

Figure 6 shows another ICR which is located again at the boundary of the hole-joining and cleavage fracture regions in a specimen from the air-quenched, entirely polygonal ferrite microstructure. In this case, the ICR was over 100 microns in diameter, and possessed a distinct fracture origin shown in Fig. 7, which is a zone of hole-joining fracture. To determine microstructural constituents of this cleavage fracture origin, this ICR was sectioned and examined with the SEM section fractographic technique described above. Figure 8 shows the substructure just adjacent to the hole-joining cleavage origin, and it can be seen that a collection of Fe_3C particles resides just below the fracture origin. The entire area beneath the ICR was densely populated with such carbides as shown in the conventional metallographic view of this ICR taken after the fracture origin was sectioned, Fig. 9. In this case, a large tempered bainite clump engulfed the ICR, and was contiguous with a region of carbide density banding. For this specimen, it was clearly established that the carbide clump participated in the cleavage fracture origin.

Figure 10 shows an ICR in an oil-quenched specimen which contained approximately 6 percent acicular ferrite. In this case, the ICR was somewhat

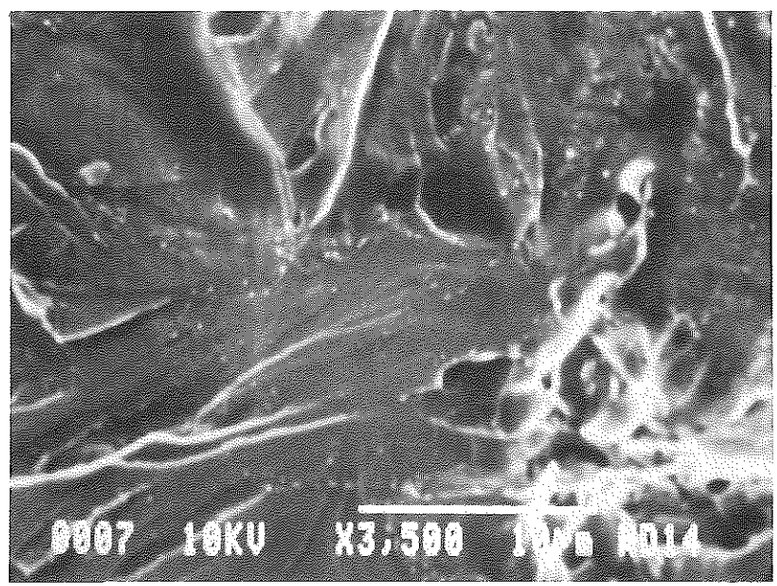

Fig 5 Scanning electron fractograph of isolated cleavage region origin in water-quenched and aged ASTM A-710 grade A steel side-grooved CVN test specimen

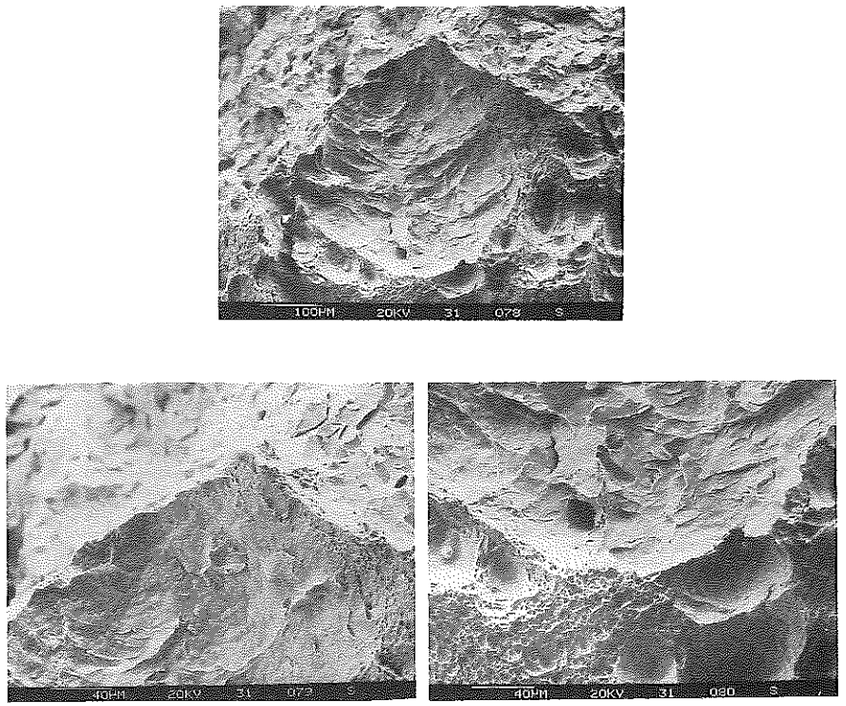

Fig 6 Scanning electron fractograph of isolated cleavage region in air-quenched and aged ASTM A-710 grade A steel side-grooved CVN test specimen

removed from the massive cleavage region and was similar to those previously reported (1)(2) in that it resided in a flat region of hole-joining and was limited in extent. As with all ICRs observed in this investigation, there was no evidence of individual particle fracture leading to the limited cleavage fracture. Rather, an accumulation of fine particles, assumed to be carbides, was identified as the origin, Fig. 10.

In summary, examination of the limited number of ICRs which were observed in all three microstructures showed that the origins of cleavage fracture stemmed from the clumps of carbides which formed during ageing in the secondary transformation product regions. The cleavage fracture surfaces showed curvatures typical of quasi-cleavage. There was no evidence that brittle separation of an individual particle (including carbides or larger manganese sulphides) triggered the onset of cleavage in this steel. These observations augmented those of Irwin *et al.* (2), and corresponded to the formulation of the model for near upper shelf fracture discussed below.

Discussion

Previous treatments of the cleavage fracture process have concentrated on large, non-crystallographic separations as the origin of the brittle cracking

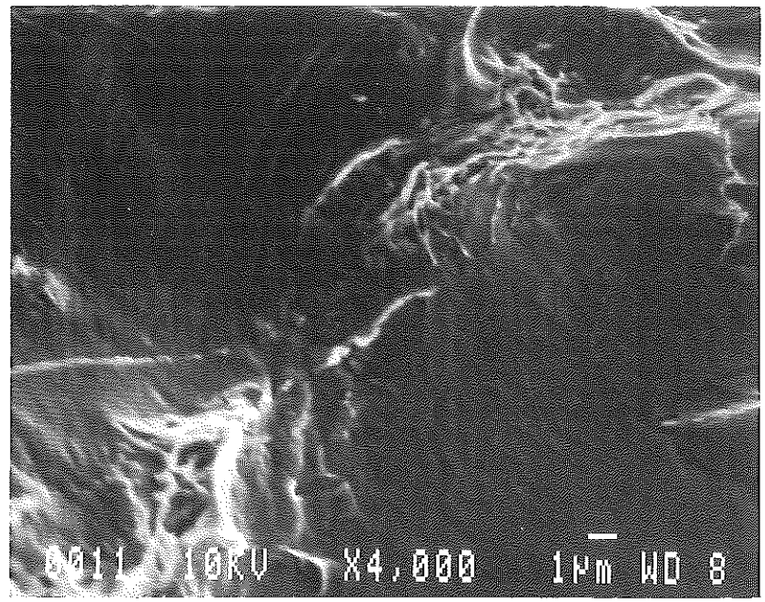

Fig 7 Scanning electron fractograph of isolated cleavage region origin in air-quenched and aged ASTM A-710 grade A steel side-grooved CVN test specimen

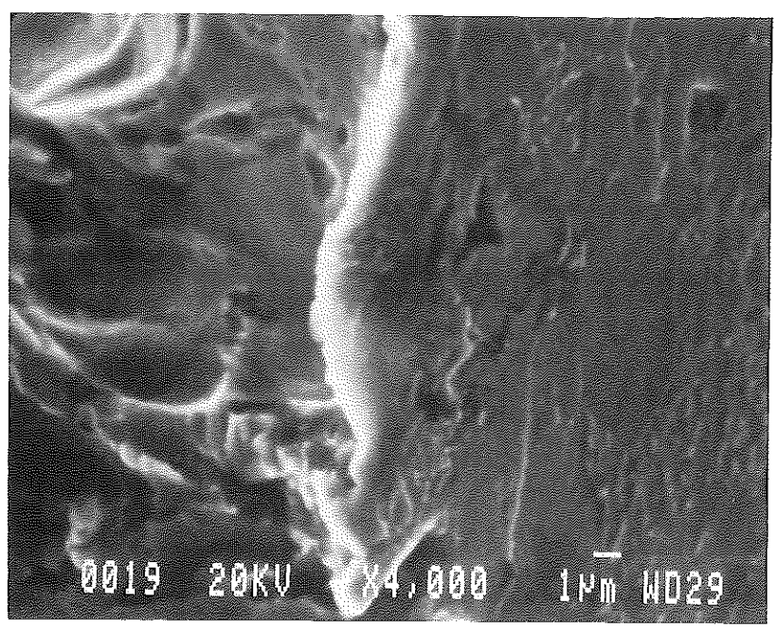

Fig 8 Scanning electron microscope section micrograph of origin of isolated cleavage region origin in air-quenched and aged ASTM A-710 grade A steel side-grooved CVN test specimen

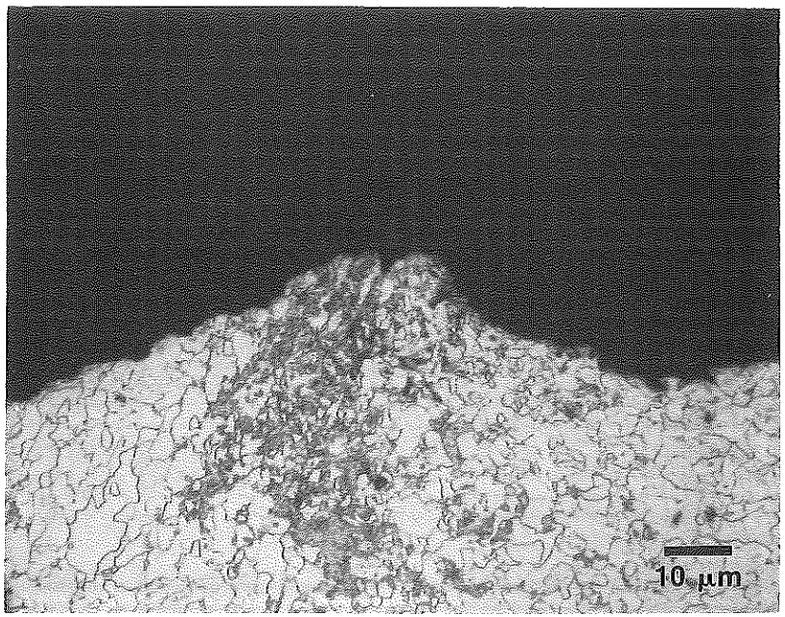

Fig 9 Optical photomicrograph of plane through isolated cleavage region origin in air-quenched and aged ASTM A-710 grade A steel side-grooved CVN test specimen

event. The results developed in this investigation point away from cracks originating in individual carbide particles as the main source of cleavage fracture. Rather, cleavage is seen to often emanate from regions which contain dense distributions of carbides in matrices of acicular or polygonal ferrite. The key element of the model produced in this study is the postulation that cleavage originates from a cleavage 'embryo' which experiences a very high stress. The stages of the model then focus on the physical events which contribute to development of very high local stress, even in a metallurgically clean and relatively homogeneous steel such as ASTM A-710.

Three stages associated with local stress elevation events are postulated. Stage I incorporates irregularities of crack growth which lead to irregularities of local strain and separation in the plastic fracture process. Such irregularities provide local regimes of high tensile stress on particle clumps. Stage II involves fast hole-joining fracture of the particle clump after small uniform strain, giving rise to a very rapid load transfer. Stage III involves spreading of cleavage from a small embryo which is crystallographic in nature. Here, the focus is the extremely high local stress necessary to cause a spreading from the cleavage embryo. Metallurgical details, such as lattice orientation relative to the direction of tension, grain size, and existence of small particles, relate to the spreading of cleavage fracture.

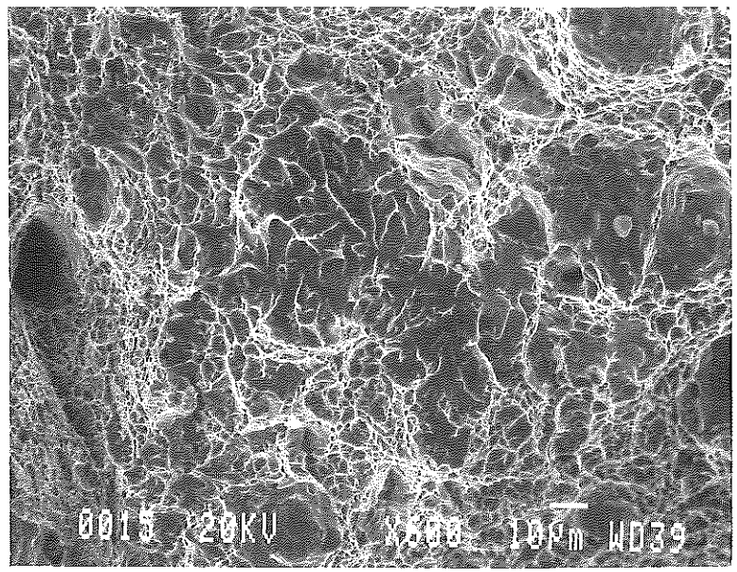

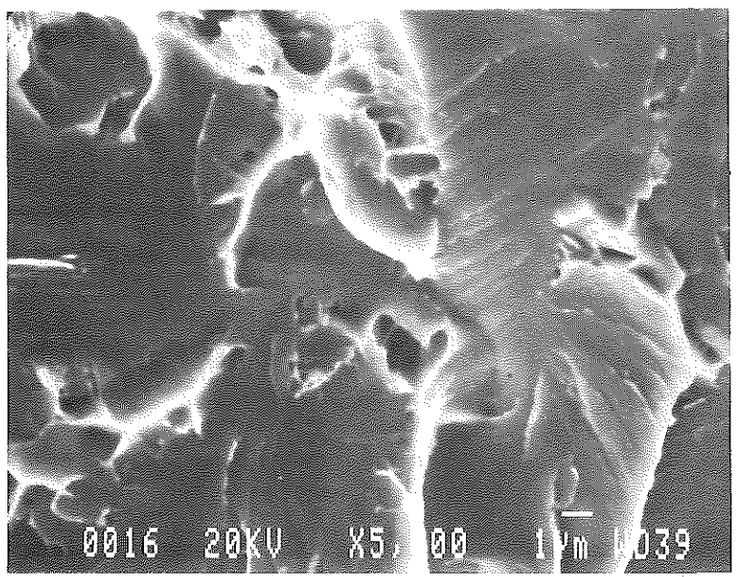

Fig 10 Scanning electron fractograph of isolated cleavage region and its origin in oil-quenched and aged ASTM A-710 grade A steel side-grooved CVN test specimen

Figure 11 is a schematic diagram of the microstructural model which has been developed to describe the initiation of cleavage at a particle clump. A main presumption is that a particle clump, when loaded rapidly, can separate sufficiently abruptly to generate a tensile stress high enough for cleavage initiation in the adjacent ferrite grain. The current ICR observations are consistent with a rare event characteristic for cleavage close to the loss of cleavage temperature because of the need for a combination of conditions to be fulfilled.

Initial stress elevation at the particle clumps occurs in response to the external loading rate as affected by the ductile crack growth speed and by the intensified plastic flow at the tip region of the ductile crack. Irregularities of microstructure lead to irregularities of local strain and separation during the ductile crack growth process. From examination of the ICRs seen in this study and the ductile/cleavage fracture interfaces, it is inferred that the size of these irregularities is on the order of 100–200 microns or greater. In this study, the fatigue precracking of CVN specimens resulted in sufficient local stress elevation to eliminate this step. However, for the case of the side-grooved specimens where fast-moving ductile crack fronts were produced, local irregularities appear to play a role.

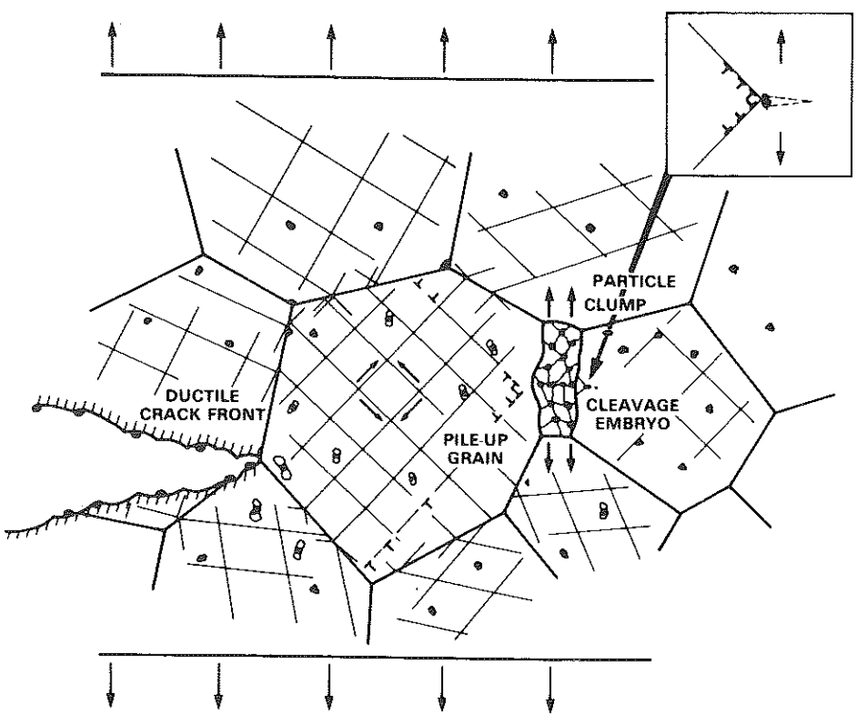

Fig 11 Elements of model of transition to cleavage from rapid co-planar hole joining

Stage II of this model is pictured as the rapid and relatively brittle fracture of the particle clump. The particle clump presents itself as a stiff carbide-strengthened region similar to pearlite. Its high strength requires a higher local tensile stress for yielding but it gives relatively small uniform plastic strain prior to onset of fast hole-joining instability. Armstrong and Zerilli **(17)** have shown the relationship between increased strength and reduced strains to tensile instability of Armco iron. Results in this study point to local hole-joining separation within the particle clump (Figs 5, 7, and 10). Load transfer from rapid separations at a very small scale occurs in times which are correspondingly very small.

Supporting evidence for the role of the particle clump in the cleavage fracture process is provided in recent investigations of heat affected zone (HAZ) fracture toughness in steels. Aihara and Haze **(18)** examined the micromechanisms of cleavage fracture associated with local brittle zones in a series of tests of simulated HAZs in several low carbon HSLA steels. They found that cleavage fracture was associated with martensitic islands, and identified microcracks at the interface between the martensite island and ferrite matrix, or in the ferrite matrix adjacent to the martensitic islands. Haze and Ahira **(19)** examined simulated HAZs produced in experimental low carbon steels. The CTOD fracture toughness was shown to have a close correlation with the volume of M–A. These authors postulated several cleavage initiation mechanisms including the stress concentration effect of the M–A island in the ferrite matrix, and Griffith cracks forming in the M–A or at the M–A/ferrite boundary.

The size of tempered M–A and tempered bainite islands produced in this study ranged from approximately 0.5 to 4 microns. The resulting high local strain rate over these local regions can produce a very high elevation of local stress which leads to stage III of the postulated fracture process which is spreading of cleavage from a very small, but crystallographic cleavage embryo which experiences very high stress.

The hole-joining fracture process has been described in terms of three stages including nucleation of voids or cavities, growth of cavities with continued deformation, and coalescence of voids comprising rupture or crack growth **(20)–(30)**. In the various models, fracture toughness is related to the spacing of holes or voids. In the previous study by Irwin of ductile fracture within carbide banded regions of ASTM A-508 steel **(31)**, planar arrays of closely spaced holes were observed with features suggestive of rapid brittle separation. Carbide density in a banded region is variable, and it is plausible to expect that the most severe degrees of rapid brittle separation would occur at the local regions of highest particle density which have been termed 'particle clumps'. If it is assumed that a high local stress elevation from stage 1 causes rapid brittle fracture of a particle clump, separation through the particle clump should occur in a time on the order of the size of the clump (assume 4 microns) divided by the speed of relatively brittle crack separation (assume 300

m/s). Clearly local strains within the border region of such a separation of several percent would be expected, and must occur in a time comparable to 0.01 microseconds. Thus, local strain rates comparable to 10^6/s are present. Discussions of the stress induced by rapid plastic straining were given by Drucker **(32)** and Freund and Hutchinson **(33)**. Both predicted rapid elevation of effective modulus when the strain rate became more than 10^5/s. Drucker suggested that a shear modulus limit of about G/40 at a strain rate approaching 10^6/s would be plausible. Converting this to a tensile deformation, the stresses adjacent to and within the border of a rapidly separated particle clump must be near E/40. This estimate is consistent with recent calculations of the high strain rate properties of Armco iron by Armstrong and Zerilli **(17)**.

To obtain an estimate of the size of a cleavage embryo which might form and connect with the particle clump fracture, assume a flat circular crack of radius, a, a normal tension of E/40, and a crack extension force of 20 J/m^2. From the equation:

$$20 \text{ J/m}^2 = (4a/\pi)(\sigma^2/E)(1 - \nu^2)$$

with $\nu = 0.3$, the value of a is 0.13 microns. This size estimate seems plausible because particles of about that size, which might form cleavage embryos by blockage of slip, are abundant in the ferrite matrix.

All models of cleavage initiation have been overly simplistic to some degree, and the model proposed here must be viewed in a similar manner. The principal differences between this and previous models are related to the initial and final events of the cleavage initiation sequence. With particular regard to cleavage initiation at temperatures above the 'lower shelf', inhomogeneities of microstructure produce substantial crack front irregularities leading to a wide range of abrupt load-transfer stress elevations. It is interesting to note that larger degrees of microstructural inhomogeneity are associated with more frequent observations of ICRs. In this study with a fine-grained ferritic steel, there were relatively few ICRs seen, whereas previous studies of nuclear pressure vessel steels and weldments **(1)–(3)** have produced numerous observations of these subcritical cleavage events. Thus, it is concluded that microstructural inhomogeneity plays a major role in the development of scatter in small specimen cleavage initiation toughness results as the test temperature increases above the lower shelf level.

With regard to the final event which is spreading of cleavage from a small cleavage embryo, the focus of interest is the extremely high local stress elevation necessary for such an event. Recent results of Dally *et al.* **(34)** who conducted notched round bar tensile tests of SA 508-2 steel under impact loading showed that scatter in fracture toughness at one test temperature was significantly reduced and compared well with small specimen lower bound measurements. Additionally, lattice orientation relative to the direction of tension, small particles, and heterogeneity of grain size may influence successful initiation of a spreading cleavage event. Recent work by Natishan **(35)**, for example, points up the significance of large ferrite grains in cleavage fracture initiation of ASTM A710 Grade A Class III steel. To assume that this stage of cleavage fracture has a high probability and can be neglected is not unreasonable. However, the extremely high local stress elevation causing this final event in the cleavage initiation sequence is of value relative to studies of cleavage initiation in terms of dislocation models and is obviously essential for completeness.

Summary and conclusions

The purpose of this investigation was to examine the application of the three-stage model to near upper shelf cleavage initiation in ASTM A-710 Grade A steel which was austenitised and then quenched at three different rates, followed by ageing that precipitation strengthened the ferrite and tempered the secondary transformation products. Metallographic and fractographic examination of isolated cleavage regions in precracked and side-grooved CVN specimens which experienced dynamic hole-joining fracture prior to the onset of cleavage clearly identified cleavage origins that were associated with hole-joining fracture in clumps of secondary transformation products including tempered M–A and tempered bainite constituents.

The three stage model postulated to describe the events which are required to trigger fracture in the near upper shelf regime included the following elements:

(i) irregularities of abrupt plastic deformation and separation which provide local regimes of high tensile stress on particles or particle clumps;
(ii) unstable, fast hole-joining fracture of the particle or particle clump after small uniform strain, giving very rapid load transfer;
(iii) spreading of cleavage from an adjacent small cleavage embryo which experiences extremely high normal stress.

Grain size and crystallographic orientation must play a role in both stage (i) and stage (iii) of this fracture process.

It is concluded that this three stage model appropriately addresses the rare event nature of cleavage initiation in the upper transition regime of fracture. Results of this study directly point to the role of secondary transformation particle clumps in the initiation of the cleavage fracture process and emphasise the requirement for local stress elevation. In the context of this model, the role of microstructural homogeneity is seen as key to preventing cleavage fracture in the regime where ductile fracturing would normally be expected.

Acknowledgements

The authors gratefully acknowledge the helpful discussions of Dr Thomas Scoonover and assistance of Messrs Jack Saveleski and Albert Brandemarte of the David Taylor Research Center. Frau Monika Aberham, Herr Siegfried Winkler, Herr Josef Schuler, and Dr Bert Voss of the Fraunhofer-Institute für

Werkstoffmechanik, Freiburg, Federal Republic of Germany, provided valuable support during the conduct of the tests.

References

(1) ZHANG, X. J., ARMSTRONG, R. W., and IRWIN, G. R. (1986) *J. Mat. Sci. Letts*, **5**, 961–964.
(2) IRWIN, G. R., ZHANG, X. J., and ARMSTRONG, R. W. (1989) *J. Mat. Sci. Letts*, **8**, 844–848.
(3) ZHANG, X. J., ARMSTRONG, R. W., and IRWIN, G. R. (1989) *Met. Trans*, **20A**, pp. 2862–2868.
(4) McMAHON, C. J. and COHEN, M. (1965) *Acta Met.*, **13**, 591–604.
(5) SMITH, E. (1966) *Proceedings of Conference on Physical Basis of Yield and Fracture*, Institute of Physics and The Physical Society, Oxford, pp. 36–46.
(6) KNOTT, J. F. (1966) *J.* Iron *Steel Inst.*, **204**, 104–111.
(7) RITCHIE, R. O., KNOTT, J. F., and RICE, J. R. (1973) *J. Mech. Phys Solids*, **21**, 395–410.
(8) CURRY, D. A. and KNOTT, J. F. (1976) *Met. Sci.*, **10**, 1–6.
(9) CURRY, D. A. and KNOTT, J. F. (1978) *Met. Sci.*, **12**, 511–514.
(10) CURRY, D. A. and KNOTT, J. F. (1979) *Met. Sci.*, **13**, 341–345.
(11) WALLIN, K., SAARIO, T., and TORRONEN, K. (1984) *Met. Sci.*, **18**, 13–16.
(12) SAARIO, T., WALLIN, K., and TORRONEN, K. (1984) *J. Engng Mater. Technol.*, **106**, 173–177.
(13) EVANS, A. G. (1983) *Met. Trans*, **14A**, 1349–1355.
(14) LIN, T., EVANS, A. G., and RITCHIE, R. O. (1987) *Met. Trans*, **18A**, 641–651.
(15) PETCH, N. J. and ARMSTRONG, R. W. (1989) *Acta Met.*, **37**, 2279–2285.
(16) SPEICH, G. R. and SCOONOVER, T. M. (1988) *Processing, microstructure and properties of HSLA steels* (Edited by A. J. DeArdo), The Minerals, Metals, and Materials Society, pp. 263–286.
(17) ARMSTRONG, R. W. and ZERILLI, F. J. Presented at ASME Conference on Constitutive Modeling of Engineering Materials, San Francisco, California, to be published.
(18) AIHARA, S. and HAZE, T. (1988) presented at TMS annual meeting, Phoenix, Arizona.
(19) HAZE, T. and AIHARA, S. (1988) *Proceedings of Seventh Int. Conf. on Offshore Mech. and Arctic Enging*, Houston, TX, pp. 515–523.
(20) ROSENFIELD, A. R. (1968) *Met. Rev.*, **13**, 29–40.
(21) HAHN, G. T. (1976) *Atomic Structure and Mechanical Properties of Metals*, North Holland, Amsterdam and New York, pp. 436–490.
(22) HAHN, G. T. and FLANAGAN, W. F. (1980) *Proceedings of Conf. on Dislocation Modelling of Physical Systems*, Gainsville, Florida, pp. 1–17.
(23) KNOTT, J. F. (1978) *Proceedings of the Fourth Int. Conf. on Fracture* (Edited by D. M. R. Taplin), Pergamon Press, New York, pp. 61–92.
(24) KNOTT, J. F. (1980) *Metal Science*, **14**, 327–336.
(25) KNOTT, J. F. (1982) *Proceedings of the Int. Conf. on Advances in the Phys. Metallurgy and Appl. of Steels*, The Metals Society, London, pp. 181–198.
(26) KNOTT, J. F. (1983) *Proceedings of the Conf. on Steels for Pipeline and Fittings*, The Metals Society, London, pp. 79–89.
(27) PINEAU, A. (1981) *Advances in Fracture Research* (Edited by D. Francois), Pergamon Press, New York, Vol. 1, pp. 553–577.
(28) RITCHIE, R. O. and THOMPSON, A. W. (1985) *Met. Trans*, **16A**, 233–248.
(29) WILSDORF, H. G. F. (1983) *Mater. Sci. Engng*, **59**, 1–39.
(30) VAN STONE, R. H., COX, T. B., LOW, J. R. Jr., and PSOIDA, J. A. (1985) *Int. Met. Rev.*, **30**, 157–179.
(31) IRWIN, G. R. (1987) *Proceedings of 14th Water Reactor Safety Research Inf. Meeting*, U.S. Nuclear Regulatory Commission, NUREG/CP-0082, vol. 2, pp. 251–272.
(32) DRUCKER, D. C. (1987) *Proceedings of 1985 Iutam Symposium on MMMHVDF*, Springer Verlag, Berlin, pp. 137–148.
(33) FREUND, L. B. and HUTCHINSON, J. W. (1985) *J. Mech. Phys Solids*, **33**, 169–191.
(34) DALLY, J. J., ZHANG, X. J., and IRWIN, G. R. (1989) Symposium, *Dynamic Fracture Mechanics for the 1990's*, (Edited by D. A. Shockley and G. Yagawa), ASME, **160**, pp. 47–54.
(35) NATISHAN, M. E. (1989) PhD Dissertation, University of Virginia.